Angular Dependence of Magnetic Normal Modes in NiFe Antidot Lattices With Different Lattice Symmetry

Article *in* IEEE Transactions on Magnetics · July 2010

Impact Factor: 1.39 · DOI: 10.1109/TMAG.2009.2039775 · Source: IEEE Xplore

Angular Dependence of Magnetic Normal Modes in NiFe Antidot Lattices With Different Lattice Symmetry

Silvia Tacchi[1], Marco Madami[1], Gianluca Gubbiotti[1], Giovanni Carlotti[2], Adekunle O. Adeyeye[3], Sebastian Neusser[4], Bernhard Botters[4], and Dirk Grundler[4]

[1]CNISM, Unità di Perugia, Dipartimento di Fisica, Via A. Pascoli, I-06123 Perugia, Italy
[2]Università di Perugia and CNISM, Unità di Perugia, Dipartimento di Fisica, Via A. Pascoli, I-06123 Perugia, Italy
[3]Department of Electrical and Computer Engineering, National University of Singapore, 117576 Singapore
[4]Physik Department, Lehrstuhl für Physik funktionaler Schichtsysteme, Technische Universität München, D-85747 Garching b. München, Germany

We report an experimental investigation of the magnetic normal modes in large-area $Ni_{80}Fe_{20}$ antidot arrays fabricated on commercially available silicon substrates using deep ultraviolet lithography at 248 nm exposing wavelength. The effect of the lattice symmetry (square, rhombic and honeycomb) on the magnetic normal modes of the arrays has been investigated by both Brillouin light scattering and broadband ferromagnetic resonance using a vector network analyzer. For all the measured samples, the eigenfrequencies show an angular symmetry which is consistent with the lattice arrangement of the holes. Interpretation of the experimental results was achieved by micromagnetic simulations which enabled us to calculate both the frequencies of the modes and the corresponding spatial profile, correlating their angular evolution with the magnetic ground state.

***Index Terms*—Brillouin light scattering, ferromagnetic resonance, patterned magnetic films, spin waves.**

I. Introduction

FERROMAGNETIC antidot structures where a periodic array of holes is fabricated into a continuous magnetic film, have attracted an increasing interest from both a fundamental and a technological viewpoint [1], [2]. Such a structure can be regarded as an example of a two-dimensional artificial magnonic crystal where propagating spin waves are used to transmit and process information without the use of electric current [3], [4]. Since the wavelength of magnonic excitations are shorter than those of light in the GHz range, magnonic materials offer better prospects for miniaturization at these frequencies and recently emerged as a promising research topic [5]. In a previous paper [6], we measured the spin wave dispersion in squared antidot array and interpreted it in terms of a network of magnonic waveguides, i.e. the antidot lattice was considered to consist of two families of perpendicular stripes having an effective width equal to the distance between neighboring hole edges.

In this paper, we report an experimental investigation of the spin dynamics in large-area $Ni_{80}Fe_{20}$ antidot arrays (Fig. 1) with particular emphasis on the effect of the lattice symmetry (square, rhombic and honeycomb) on the magnetic normal modes of the arrays. In particular, we investigate how the spin wave spectrum is modified by rotating the in-plane direction of the applied magnetic field H_{ext}.

Manuscript received October 28, 2009; revised December 09, 2009; accepted December 25, 2009. Current version published May 19, 2010. Corresponding author: G. Gubbiotti (e-mail: gubbiotti@fisica.unipg.it).

Color versions of one or more of the figures in this paper are available online at http://ieeexplore.ieee.org.

Digital Object Identifier 10.1109/TMAG.2009.2039775

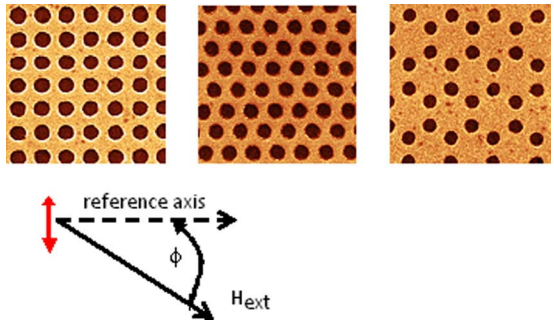

Fig. 1. Scanning electron microscopy images of the antidot arrays with square (left), rhombic (center) and honeycomb (right) lattice symmetry. The chosen coordinate system defines the in-plane angle ϕ between the external magnetic field H_{ext} and the reference direction indicated by the dashed arrow. The center-to-center spacing of nearest-neighboring holes is 400 nm in all the three different arrays.

II. Experimental Setup

Large-area $Ni_{80}Fe_{20}$ antidot structures were fabricated on commercially available silicon substrates using deep ultraviolet lithography at 248 nm exposing wavelength. To create patterns in the resist, the substrate was coated with a 60 nm thick anti-reflective layer followed by a 480 nm positive deep UV photoresist, which is four to five times thicker than those used typically in electron beam lithography. This allows one to fabricate antidots with high aspect ratio and makes the lift-off process easier. A Nikon lithographic scanner with KrF excimer laser radiation was used to expose the resist. To convert the resist patterns into antidots, 30 nm thick $Ni_{80}Fe_{20}$ was deposited using the electron beam evaporation technique at a rate of 0.2 Å/s. The pressure was maintained at 2×10^{-6} Torr during the deposition at room temperature. Lift-off processing of the deposited film was carried out in isopropyl alcohol.

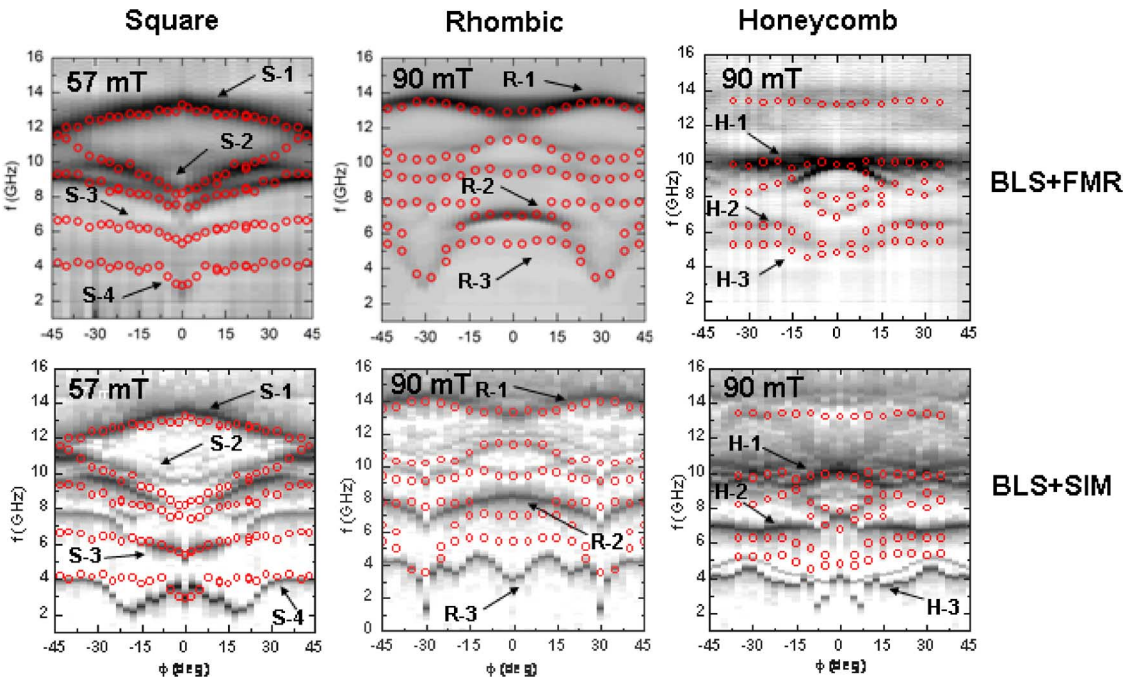

Fig. 2. (Top row) Measured microwave power absorption spectra (gray-scale plots) and BLS frequency data (red circles) as a function of the angle ϕ. For the squared antidot lattice the external field is $\mu_0 \mathrm{H_{ext}} = 57\ \mathrm{mT}$ while for the other lattices we have $\mu_0 \mathrm{H_{ext}} = 90\ \mathrm{mT}$ (Bottom row) Comparison between the experimental BLS data and simulated (SIM) spectra (gray-scale plots) for the corresponding field values.

Completion of the lift-off process was determined by the color contrast of the patterned $\mathrm{Ni_{80}Fe_{20}}$ area. The final structure consisted of $\mathrm{Ni_{80}Fe_{20}}$ arrays of antidots of diameter 250 nm. The center-to-center spacing between nearest holes was designed to be 400 nm. The holes were arranged into a square, rhombic and honeycomb lattice geometry, as shown in the scanning electron microscopy (SEM) images in Fig. 1. The spectra of magnetic normal modes were measured by both Brillouin light scattering (BLS) and broadband ferromagnetic resonance (FMR) using a vector network analyzer (VNA).

In order to directly compare frequencies measured by BLS with those obtained by VNA-FMR, the incident light was normal to the sample plane, so that spin waves with zero wavevector were probed. It is important to recall that VNA-FMR measures the resonant dynamic response of a magnetic system by sweeping the frequency of the exciting rf field while BLS detects thermally excited spin waves. Interpretation of the experimental results was achieved by micromagnetic simulations [7] which enabled us to calculate the eigenfrequencies and the spatial profiles of the corresponding modes, correlating their angular evolution with the magnetic ground state. To model the antidot lattice, two-dimensional periodic boundary conditions and one nonmagnetic hole centered in a unit cell of area $400 \times 400\ \mathrm{nm}^2$ were taken into account [8]. To excite the spin waves, a field pulse $\mathrm{h_{rf}}$ of 3 ps duration and amplitude of 4 mT was used. It was directed 45° out of plane with respect to the sample plane.

III. Results and Discussion

In Fig. 2 we compare the VNA-FMR and BLS frequencies measured by varying the in-plane orientation of the magnetic field $\mathrm{H_{ext}}$, i.e., the angle ϕ, for the three antidot lattices (top row). Both techniques reveal rich spectra. A very good agreement between VNA-FMR and BLS results is observed in the whole angular range investigated. BLS is found to be more sensitive to the lowest-frequency modes where the signal detected by the VNA-FMR technique is almost vanishing.

Spectra extracted from simulations are depicted as gray-scale plots also in Fig. 2 (bottom row). BLS data are shown again and overlaid for comparison.

As a general comment, we can say that, for all the samples, the calculated spectra reproduce the experimental results both in a qualitative and quantitative way with exception of the lowest frequency modes. This discrepancy is probably due to difficulty of reproducing the details of the real shape of the holes on the micro scale (taking into account roughness) and the internal magnetic field experienced by precessing spins in the close proximity of the hole edges.

Let us now analyse in more detail the spin-wave modes observed in the different geometries.

In the square lattice the spin-wave frequencies exhibit an in-plane four-fold anisotropy induced by the symmetry of the holes array. We notice that the frequency of the highest-frequency mode S-1 decreases as soon as the in-plane angle ϕ is turned away from zero. The decrease with ϕ is in contrast to what happens for lower lying modes whose frequencies either increase or remain almost constant in the angular range investigated. The spatial distribution of spin precession amplitudes of selected modes are shown in Fig. 3. S-1 is found to locate in the vertical region enclosed between nearest neighboring holes. When the external field is rotated, the spatial profile of this mode undergoes only a small deformation, while its frequency decreases by about 2 GHz, because of the reduction of the internal field in the sample region where it is localized.

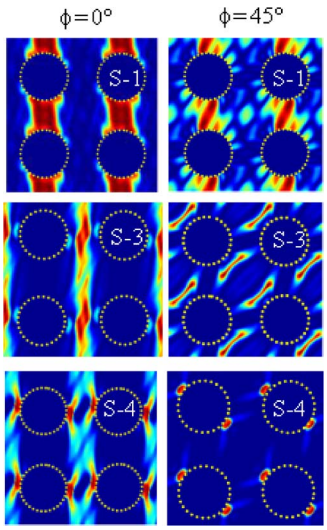

Fig. 3. Spatial distribution of spin precession amplitudes for the squared antidot array. Profiles for selected modes calculated at $\mu_0 H_{ext} = 57\ \mathrm{mT}$ and $\phi = 0°$ and 45°. Red (blue) color indicates a large (vanishing) spin precession amplitude.

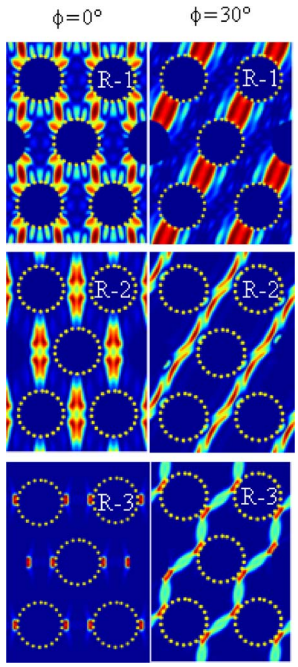

Fig. 4. Spatial distribution of spin precession amplitudes for the rhombic antidot array. Profiles for some selected modes calculated at $\mu_0 H_{ext} = 90\ \mathrm{mT}$ and ϕ of 0° and 30°. Red (blue) color indicates a large (vanishing) spin precession amplitude.

The opposite behavior, i.e. an increase of about 3.5 GHz when ϕ increases from zero to 45° is observed for the mode S-2 (not shown in Fig. 3). This mode is localized between next-nearest neighboring holes for $\phi = 0$ and exhibits a complicated spatial profile because of hybridization effects with the higher frequency mode when ϕ approaches 45°. The mode S-3, instead, for $\phi = 0$ extends through the whole lattice along the vertical stripes enclosed between the holes. When the direction of the external field is rotated, the spatial profile of the mode changes significantly. In particular we find that for $\phi > 10°$ the mode does not have the extended profile any longer, but becomes localized in the region between next-nearest neighboring holes. Mode S-4 is found to be localized at the edges of the holes where the internal field is very low due to the large value of the demagnetization field. This mode follows the position of the local magnetic poles, i.e. its position rotates when the orientation of $\mathrm{H_{ext}}$ is varied.

Concerning the rhombic antidot lattice, the frequencies measured as a function of the in-plane field orientation reflect a six-fold anisotropy, induced by the symmetry of the hole array. We observe two pronounced modes, one at about 13.0 GHz (mode R-1) and one at about 7.0 GHz (mode R-2). In addition, some other weaker peaks are visible in the range between 8 and 11 GHz and at low frequency. In Fig. 4 the simulated spatial profiles of selected modes are depicted. We found that the more intense peaks in the spectra correspond to the modes located in the regions where the static magnetization is parallel to the applied field. At $\phi = 0$ these modes reside in the vertical area, enclosed between nearest (R-1) and next-nearest (R-2) neighboring holes, respectively. When the direction of the external field is rotated, these modes accordingly move to remain in the regions where the static magnetization is aligned with the field. In particular at $\phi = 30°$, mode R-1 localizes between nearest-neighbouring holes, while R-2 becomes an extended mode which spreads along the permalloy stripes, enclosed between the holes. The low frequency mode (R-3) is the edge mode localized at the edges of the holes where the internal field is very low. This mode follows the position of the local magnetic poles; when the external field is rotated also its position rotates and acquires an extended spatial profile.

Eventually, the eigenfrequencies measured on the honeycomb lattice exhibit a six-fold in-plane anisotropy. In this case, however, eigenfrequency variations with ϕ are less pronounced if compared to both the square and the rhombic array. We explain this by the reduced density of holes in the honeycomb lattice, leading to continuous portions of NiFe at the centre of the lattice unit cell. Such areas of NiFe exhibit negligible magnetocrystalline anisotropy and experience a reduced demagnetization effect if compared to the two further lattices provoking almost constant eigenfrequencies as a function of ϕ. In Fig. 5 we show the calculated spin precession amplitudes for modes H-1, H-2 and H3 at $\phi = 0$ and $-30°$. H-1 and H-2, corresponding to the more pronounced peaks in the spectra, reside in the area where the static magnetization is aligned with the magnetic field. The mode H-1 has always a stationary character with large spin amplitude concentrated at the center of the hexagonal unit cell, independently from the orientation of the external field, while the H-2 mode has an extended character for both field orientations. Finally we find that H-3 is the edge-mode localized at the edges of the holes.

To complete our analysis, we have also carried out BLS measurements as a function of the transferred wavevector (not shown here due to length restrictions). Interestingly, it was found that some modes exhibit a dispersive character when the field is applied along lattice directions where continuous portions of NiFe are present. We attribute this character, typical of propagating waves, to modes which have been found by the micromagnetic simulations to extend through the lattice, such

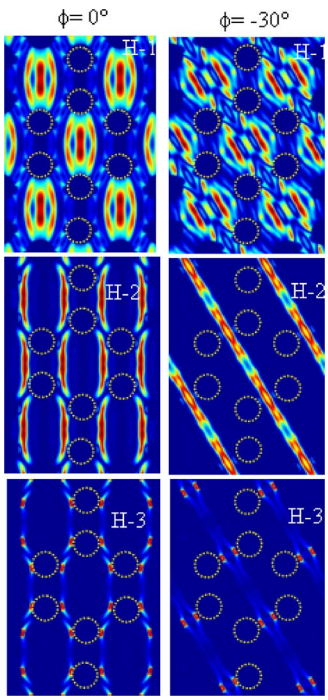

Fig. 5. Spatial distribution of spin precession amplitudes for the honeycomb antidot array. Profiles for selected modes calculated at $\mu_0 H_{ext} = 90\ \mathrm{mT}$ and $\phi = 0°$ and $-30°$ are presented. Red (blue) color indicates a large (vanishing) spin precession amplitude.

as modes S-3, S-4 and R1 for $\phi = 0$, R-2 and R-3 for $\phi = 30°$. This is because of interconnecting regions characterized by a large spin precession amplitude between neighboring holes. For examples, S-4 mode for the squared lattice and R-1 mode for the rhombic one are dispersive modes propagating along the edges and at the centre of effective magnetic stripes, respectively. Such stripes have a width equal to the edge-to-edge separation between parallel rows of holes and an orientation either perpendicular or parallel to the applied field direction.

IV. Conclusions

In this work, we have reported a systematic experimental investigation of the spin-wave modes in three different NiFe antidot lattices with squared, rhombic and hexagonal lattice symmetry. We used two different experimental techniques, namely BLS and VNA-FMR, to investigate the modes existing inside the antidot arrays as a function of the in-plane field direction. Calculations of both the frequency and spatial profiles of the modes have been performed by means of micromagnetic simulations carried out using periodic boundary condition. For all the investigated samples, the spin-wave frequencies exhibit an in-plane anisotropy induced by the symmetry of the hole array. We have also shown that the character of some modes changes from localized to extended and vice versa depending on the in-plane direction of the external applied field. We believe that our findings could be important in the contest of the present efforts to understand spin-wave propagation in the emerging field of magnonic crystals.

Acknowledgment

The research leading to these results has received funding from the European Community's Seventh Framework Programme (FP7/2007-2013) under Grant Agreement no. 228673 (MAGNONICS). This work was also supported by the Ministero Italiano per la Ricerca e l'Università under PRIN-2007 project (Prot. Grant No. 2007X3Y2Y2)

References

[1] O. N. Martyanov, V. F. Yudanov, R. N. Lee, S. A. Nepijko, H. J. Elmers, R. Hertel, C. M. Schneider, and G. Schönhense, "Ferromagnetic resonance study of thin film antidot arrays: Experiment and micromagnetic Simulations," *Phys. Rev. B*, vol. 75, p. 174429, 2007.

[2] M. Vázquez, K. R. Pirota, D. Navas, A. Asenjo, M. Hernández-Vélez, P. Prieto, and J. M. Sanz, "Ordered magnetic nanohole and antidot arrays prepared through replication from anodic alumina templates," *J. Magn. Magn. Mater.*, vol. 320, p. 1978, 2008.

[3] A. Khitun, M. Bao, and K. L. Wang, "Spin wave magnetic nanofabric: A new approach to spin-based logic circuitry," *IEEE Trans. Magn.*, vol. 44, p. 2141, 2008.

[4] T. Schneider, A. A. Serga, B. Leven, B. Hillebrands, R. L. Stamps, and M. P. Kostylev, "Realization of spin-wave logic gates," *Appl. Phys. Lett.*, vol. 92, p. 022505, 2008.

[5] S. Neusser and D. Grundler, "Magnonics spin wave on the nanoscale," *Adv. Mater.*, vol. 21, p. 2927, 2009.

[6] S. Tacchi, M. Madami, G. Gubbiotti, G. Carlotti, A. O. Adeyeye, S. Neusser, B. Botters, and D. Grundler, "Magnetic normal modes in squared antidot array with circular holes: A combined Brillouin light scattering and broadband ferromagnetic resonance study," *IEEE Trans. Magn.*, vol. 46, p. 172, 2010.

[7] [Online]. Available: www.micromagus.com

[8] S. Neusser, B. Botters, and D. Grundler, "Localization, confinement, and field-controlled propagation of spin waves in antidot lattices," *Phys. Rev. B*, vol. 78, p. 054406, 2008.